



# Depth-resolved studies of layered magnetic nanostructures using $^{57}\text{Fe}$ probe layers and Mössbauer spectroscopy

Waldemar A.A. Macedo\*

Laboratório de Física Aplicada, Centro de Desenvolvimento da Tecnologia Nuclear, 31270-901 Belo Horizonte, MG, Brazil

## ARTICLE INFO

### Article history:

Received 14 January 2014

Received in revised form

26 March 2014

Accepted 8 April 2014

### Keywords:

Magnetic multilayers  
Mössbauer spectroscopy  
Depth selectivity  
Exchange bias  
Spin structure  
Interfaces

## ABSTRACT

An atomic-scale quantitative analysis of the structural and magnetic properties of surfaces, interfaces and complex nanostructures is of fundamental relevance for the development of new materials for spintronics. Studies of buried magnetic interfaces and depth-resolved measurements in layered magnetic nanostructures are particularly challenging, and the combination of conversion electron Mössbauer spectroscopy and/or nuclear resonant scattering of synchrotron radiation with isotope-enriched probe layers can be a powerful tool in this field.

The potential offered by the application of isotope-selective measurements for the study of Fe-based layered magnetic nanostructures is illustrated with our recent results on the investigation of depth-dependent spin structures and interfacial interdiffusion in exchange-biased ferromagnetic/antiferromagnetic bilayer systems and of an epitaxial magnetic system with perpendicular magnetic anisotropy, obtained from samples prepared with ultrathin  $^{57}\text{Fe}$  probe layers placed at different depths during the growth processes, via molecular beam epitaxy or sputtering deposition.

© 2014 Elsevier B.V. All rights reserved.

## 1. Introduction

For the development of new materials for spintronics, it is of fundamental relevance a detailed quantitative analysis of the structural and magnetic properties at surfaces, interfaces and along complex nanostructures, in an atomic scale [1]. In layered magnetic systems, there is a need for depth-dependent measurements, providing access to the study of buried magnetic interfaces. There are different experimental techniques that allow depth-dependent characterization of both structural and magnetic properties, including neutron scattering and reflectometry, magnetic dichroism (XMCD), Mössbauer spectroscopy (MS), nuclear resonant scattering of synchrotron radiation (NRS), soft X-ray resonant Kerr rotation, soft X-ray resonant magnetic scattering. Among these techniques, isotope selective methods, like MS and NRS, offer a specific advantage, additional to chemical element selectivity, namely the possibility of separating out contributions coming from different crystallographic sites occupied by the same element. Depth-resolved measurements in layered magnetic nanostructures are particularly challenging, and the combination of conversion electron Mössbauer spectroscopy (CEMS) and/or NRS associated with the adequate growth of isotope-enriched probe layers allows a depth resolution of few Angstroms (monolayer (ML) regime), measurements on surfaces and on buried

interfaces, the determination of the spin and local structure, degree of interdiffusion, and interface roughness on an atomic scale, being a very effective approach for the investigation of layered magnetic nanostructures, and, therefore, a powerful tool in this research field [2–7]. The recent developments in synchrotron-radiation-based MS in the energy domain add also new possibilities for the area [8].

In this paper, some of our recent results illustrating the potential offered by CEMS and NRS for the study of Fe-based layered magnetic nanostructures are reviewed. The focus is more specifically on depth-resolved studies using  $^{57}\text{Fe}$  probe layers and isotope-selective measurements. The applications of these techniques is illustrated with our results on the investigation of depth-dependent spin structures, of interfacial interdiffusion in exchange-biased ferromagnetic (F)/antiferromagnetic (AF) bilayer systems, and of epitaxial magnetic systems with perpendicular magnetic anisotropy, obtained from samples prepared with ultrathin (a few Angstroms thick)  $^{57}\text{Fe}$  probe layers placed at different depths during the growth processes, via molecular beam epitaxy or sputtering deposition.

## 2. Spin structure during magnetization reversal in Fe/MnF<sub>2</sub> exchange-coupled bilayers

We measured directly the depth-dependent Fe spin rotation upon magnetization reversal in exchange-coupled Fe/MnF<sub>2</sub> bilayers using nuclear resonant scattering of synchrotron radiation

\* Tel.: +553130693370.

E-mail address: [wmacedo@cdtn.br](mailto:wmacedo@cdtn.br)

from a  $^{57}\text{Fe}$ -probe layer buried at different depths within the Fe film. Our results showed that the exchange-biased ferromagnetic layer develops a non-collinear spin structure along the film normal direction, reminiscent of a partial domain wall parallel to the Fe/MnF<sub>2</sub> interface [9].

The exchange bias (EB) effect, originating from the interface coupling between a F and an AF, gives rise to shifted hysteresis loop along the magnetic field ( $x$ -) axis [10–13]. This effect is used to set a reference magnetization direction in layered spin-valve devices and, therefore, is of great interest for many applications based on spintronics [1,14]. Despite the enormous technological impact and the intense research efforts, one of the main challenges to understand the microscopic mechanisms of EB is the investigation of the magnetic structure at the F/AF interface and its depth dependence perpendicular to the interface. Some EB models predict a spiraling AF spin structure perpendicular to the interface, and non-collinear spin structures in the F layer [12,15–18], but systematic experimental studies on that aspects are scarce [19,20].

Although different techniques allow the study of buried magnetic interfaces, experimentally, it is always difficult and challenging to obtain a detailed description of the depth dependent magnetic structure at the atomic scale. Previous conversion electron Mössbauer spectroscopy (CEMS) studies using  $^{57}\text{Fe}$  probe layers at different depths of the F in exchange-biased Fe/MnF<sub>2</sub> did not indicate depth-dependent spin structure in Fe [21,22]. However, due to the inherent difficulties of detecting electrons while applying strong external magnetic fields, these CEMS measurements were conducted in remanence [21,22].

For Fe-containing nanostructures, the use of coherent nuclear resonant scattering (NRS) of synchrotron radiation technique with buried ultrathin (a few Angstroms thick)  $^{57}\text{Fe}$ -rich probe layers in combination with wedge-type Mössbauer inactive  $^{56}\text{Fe}$  layers, is a powerful approach to access depth-dependent properties in magnetic films and multilayers, with high sensitivity and high lateral resolution [23,24]. We applied NRS to conduct direct measurements of the depth-dependent Fe spin rotation in an exchange-coupled Fe/MnF<sub>2</sub> bilayer [9]. A SQUID magnetization loop at 10 K for such F/AF bilayer is shown in Fig. 1, where an exchange bias field (horizontal shift,  $H_E$ ) of  $-80$  Oe is observed.

The Fe/MnF<sub>2</sub> sample of 40 Å Cu cap/70 Å Fe (60 Å  $^{56}\text{Fe}$  + 10 Å  $^{57}\text{Fe}$  wedge)/520 Å MnF<sub>2</sub>(1 1 0)/160 Å ZnF<sub>2</sub>(1 1 0) buffer layer was grown on MgO(1 0 0) [21]. The 10-Å thick  $^{57}\text{Fe}$  probe layer (95.5% enrichment) was inserted between two  $^{56}\text{Fe}$  wedges, as illustrated in Fig. 2(a), together with geometry details of the NRS experiments. The MnF<sub>2</sub> film grows as a quasiepitaxial layer with (1 1 0) orientation, and forms a compensated AF surface with the Mn spins in the interface plane, and the Fe layer is polycrystalline [21]. CEMS results (not shown) indicate a fully in-plane magnetized

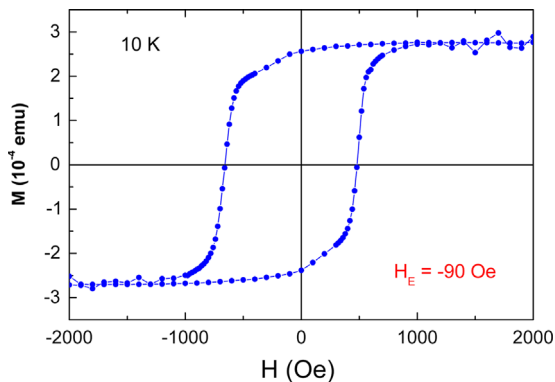


Fig. 1. SQUID magnetization loop at 10 K for a 70 Å Fe +  $^{57}\text{Fe}$ /520 Å MnF<sub>2</sub> sample, after field cooling in a magnetic field of 2.0 kOe applied along the MgO[0 0 1] direction, from 150 K (adapted from Ref. [9]).

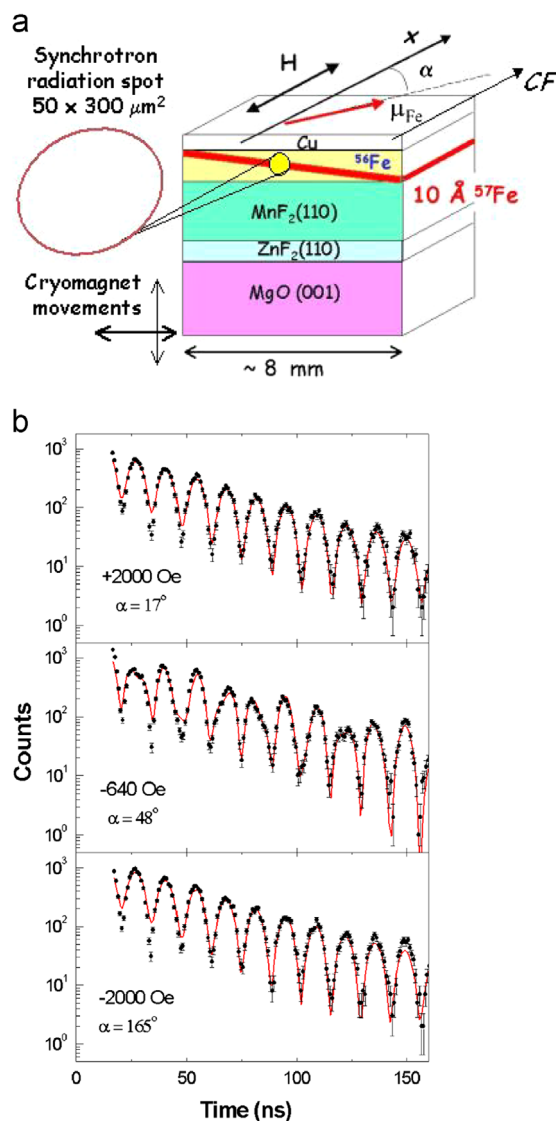


Fig. 2. (a) Schematic illustration of the wedge sample and NRS experimental geometry: the incident photon beam, reflected at an angle of 4 mrad relative to the surface, is oriented along the  $x$  direction (note that all the arrows are in the sample plane). (b) Typical 10 K NRS time spectra measured in decreasing magnetic fields with the 14.4 keV photons probing the  $^{57}\text{Fe}$  center position. The red solid lines are least-squares fits to the experimental data. The +2000 Oe cooling field (CF) (applied from 150 to 10 K) and the sweeping field  $H$  were applied in plane along the MgO[1 0 0] ( $x$ ) direction.  $\alpha$  is the angle between the in-plane Fe spin direction and the  $+x$  direction (adapted from Ref. [9]).

$^{57}\text{Fe}$  layer, in agreement with previous works [21,22]. Magnetic hysteresis loops below the MnF<sub>2</sub> Néel temperature ( $T_N=67$  K) were measured using superconducting quantum interference device (SQUID) magnetometry. EB was always established by field cooling (FC) the sample from 150 K to 10 K in an external field ( $H$ ) of 2.0 kOe applied in-plane along the MgO[0 0 1] direction ( $x$ -direction, Fig. 2(a)). Measurements were conducted between +2000 Oe and  $-2000$  Oe along the same direction, and a  $H_E$  of  $-90$  Oe was obtained at 10 K (Fig. 1).

The NRS experiments were performed at beamline ID18 of the European Synchrotron Radiation Facility (ESRF), with the 14.4 keV photon beam along the MgO[0 0 1] direction ( $x$ , Fig. 2(a)), and in grazing incidence of 4 mrad. A cryomagnet system allowed the fine adjustment and scanning of the sample in front of the  $50\ \mu\text{m}$  (vertical)  $\times$   $300\ \mu\text{m}$  (horizontal) photon beam, and, consequently, provided the depth selectivity of the measurements along the  $^{57}\text{Fe}$  wedge, by probing regions at different distances from the F/AF

interface. We explored two positions of the  $^{57}\text{Fe}$  layer: the *center* position, 24 Å away from the F/AF interface, and the *top* position, which is 60 Å away. The measurements were conducted at 10 K and at 150 K (well below and above  $T_N$  of  $\text{MnF}_2$ , respectively), and the time spectra were least-squares fit using the CONUSS program [25]. In NRS, the time response of the forward scattered intensity reflected from the ultrathin  $^{57}\text{Fe}$  probe layer is measured [23,24]. We assume the magnetization to be confined in the sample plane [21]. For the  $^{57}\text{Fe}$  resonance, the standard NRS geometry (with incident  $\sigma$ -polarization and no polarization analysis in the detection) was employed [24]. The relative orientation of the in-plane Fe magnetic moment ( $\mu_{\text{Fe}}$ ) with respect to the incident wave vector directed along  $x$  (azimuthal angle  $\alpha$ ) is determined from the time spectra [23,24], providing the same information as obtained from the line intensity ratio in conventional MS [21].

Typical 10-K NRS time spectra for selected magnetic fields along the decreasing-field branch of the hysteresis loop at the center position are shown in Fig. 2(b). As expected for bcc Fe at 10 K, a  $B_{\text{HF}}$  of  $34.1 \pm 0.2$  T was obtained from all time spectra of the *center* and *top* position in the whole applied magnetic field range. Assuming a unidirectional collinear Fe spin structure within the depth interval sensed by the X-ray beam at either position, the in-plane spin rotation angle  $\alpha$  of the Fe magnetic moment as a function of  $H$  was determined. Following this approach, NRS angular hysteresis loops can be constructed from the experimental results (for details, see Ref. [9]).

Fig. 3 shows the full 10 K NRS angular hysteresis loop for the *center* position (full blue circles) and the descending-field branch at the *top* position (full red squares). From the field-dependence of  $\alpha$  along the decreasing-field branches of the NRS loops, it is evident the depth-dependent magnetization reversal at 10 K. As pointed out, the  $^{57}\text{Fe}$  spins at the top layer (60 Å from the interface) revert  $\sim 40$  Oe earlier than the Fe spins at the center layer (24 Å from the interface), implying stronger pinning of the Fe atoms closer to the exchange-biased Fe/ $\text{MnF}_2$  interface. Moreover, at +2000 Oe, the *top* layer spins are fully aligned with the field ( $\alpha=0^\circ$ ), but the spins at the *center* layer are misaligned with respect to the field direction ( $\alpha=17^\circ$ ). The same tendency is observed at -2000 Oe. Note also that at the different depths both site-selective 10 K NRS loops are characterized by continuous rotations, followed by jumps of the Fe spin direction at  $H=-H_C$  (or  $H=+H_C$ ) from about  $\alpha=\pm 45^\circ$  (or  $\alpha=\pm 135^\circ$ ) to  $\alpha=\pm 135^\circ$  (or  $\alpha=\pm 45^\circ$ ) at magnetization reversal. In addition to the direct evidence of depth-dependent spin rotation, this is a direct

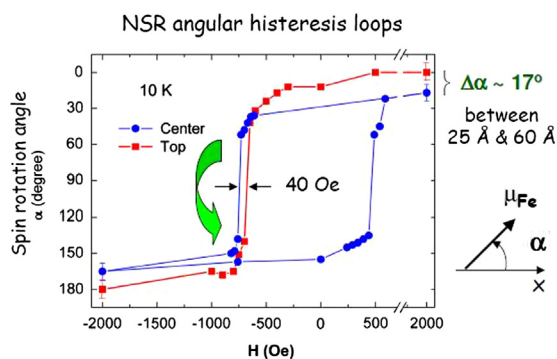


**Fig. 3.** 10 K NRS angular hysteresis loop at the  $^{57}\text{Fe}$  center position (24 Å from the Fe/ $\text{MnF}_2$  interface, blue full circles) and descending-field branch at the  $^{57}\text{Fe}$  top position (60 Å from the interface, red full squares). The depth dependence of the Fe spin structure at 10 K is reflected in the 40 Oe shift and in the different values of  $\alpha$  at  $\pm 2000$  Oe between the curves. The *center* and *top* data were measured in two independent NRS runs, after FC in +2000 Oe from 150 to 10 K. The green vertical arrow indicates the jumps upon magnetization reversal (see text) (adapted from Ref. [9]). (For interpretation of the references to color in this figure legend, the reader is referred to the web version of this article.)

observation of the fourfold magnetic anisotropy induced by the exchange interaction between the Fe and  $\text{MnF}_2$  layers [26]. This study is presented in more details in Ref. [9]. The same approach was applied recently, for example, to investigate the depth-dependent magnetization reversal of Fe/NiO exchange coupled bilayers [20].

### 3. Influence of interdiffusion on exchange bias of polycrystalline IrMn/FeCo

The influence of atomic interdiffusion as a function of the magnetic annealing temperature on exchange bias field and coercivity of polycrystalline IrMn/CoFe-based EB system was investigated by using  $^{57}\text{Fe}$  probe layers and depth-resolved conversion electron Mössbauer spectroscopy (CEMS). Our results indicated that the highest exchange bias was obtained after magnetic annealing at 450 °C, despite significant interdiffusion at the F/AF interface and along the CoFe layer [27].

For spintronic devices based on magnetic spin-valve stacks, magnetic annealing is broadly used to achieve large exchange bias field values [11].  $H_E$  depends on the magnetic field and the temperature at which the F/AF exchange interaction is set ( $T_S$ ).  $T_S$  is generally limited by the manufacturing conditions of a GMR or TMR device [28]. For systems containing IrMn, the basic AF material for the hard disk industry, different results have been reported regarding the effect of setting EB between 200 °C [29] and 400 °C [30,31]. Atomic interdiffusion is expected to have strong influence on the performance of the devices [32,33]. Also, as the thickness of the AF is reduced, the contribution of the interfacial spins becomes more significant for their performance [34]. We have investigated the influence of the magnetic annealing temperature and the consequent atomic interdiffusion on exchange bias field and coercivity of polycrystalline IrMn/CoFe bilayers [27].

Ta/( $^{57}\text{Fe}$ +CoFe)(5 nm)/IrMn(7 nm)/Ru/Ta samples were deposited on Si substrates at room temperature (RT) by magnetron sputtering. 10 Å thick  $^{57}\text{Fe}$  tracer layers were deposited at the IrMn/CoFe interface, and inside the CoFe layer, 10 Å and 20 Å above the AF/F interface, as illustrated in Fig. 4. Annealings were conducted at temperatures ranging from 225 °C to 500 °C, for 1 h, under a magnetic field of 3 kOe applied along the sample plane. The structure of the multilayer samples were characterized as-deposited and after magnetic annealing, by grazing incidence X-ray diffraction (GIXRD) and X-ray reflectivity (XRR). CEMS was used to characterize interfacial sharpness and the degree of chemical interdiffusion at different depths across the samples. Magnetic hysteresis loops were measured by vibrating sample magnetometry (VSM). As determined by GIXRD and XRR (not

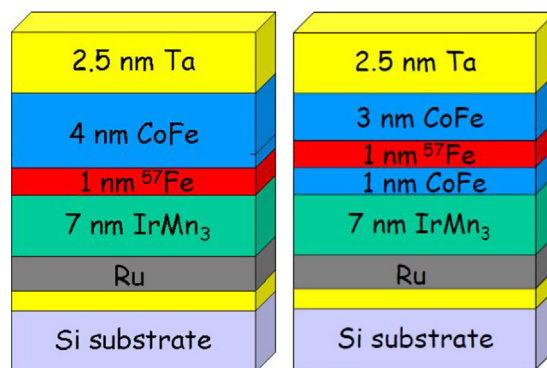


**Fig. 4.** Schematic illustration of two of the three different series of polycrystalline exchange-biased  $^{57}\text{Fe}$ +FeCo/IrMn multilayer samples prepared by magnetron sputtering deposition: (a)  $^{57}\text{Fe}$  at the interface, and (b)  $^{57}\text{Fe}$  10 Å away.



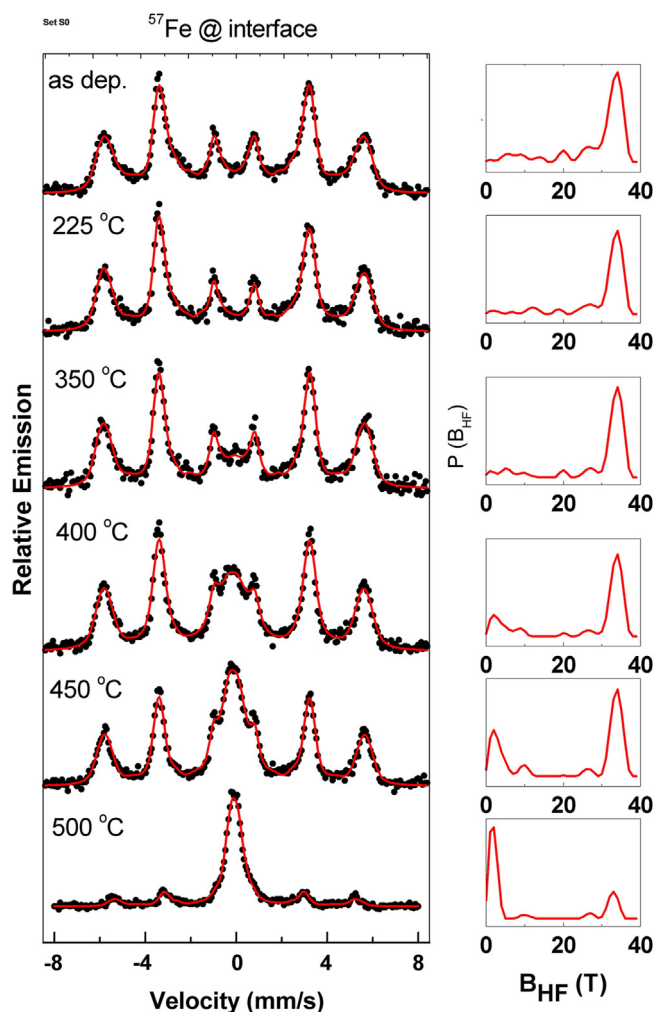


Fig. 5. RT CEM spectra for the  $^{57}\text{Fe}/\text{FeCo}/\text{IrMn}$  samples with  $^{57}\text{Fe}$  directly at the interface, and respective magnetic hyperfine field distributions  $P(B_{\text{HF}})$ . The magnetic annealing temperatures are indicated (adapted from Ref. [27]).

shown), the samples present a strong fcc (1 1 1) IrMn texture parallel to the interface, on top of hcp Ru(1 0 0). The samples presented sharp interfaces in the as-deposited state, and no detectable variation of the IrMn grain size for the different annealings.

Fig. 5 shows the RT CEM spectra for the as-deposited state (as dep.) and after the different annealings for the interface sample, together with the corresponding magnetic hyperfine field distributions ( $P(B_{\text{HF}})$ ), and Fig. 6 shows the RT CEM spectra for the samples with the  $^{57}\text{Fe}$  probe layer at 10 Å and 20 Å inside the FeCo film. In all spectra, it can be observed a high  $P(B_{\text{HF}})$  component, i.e., a distribution of sextets that represents the ferromagnetic contribution at the interface. These sextets are assigned to ferromagnetic  $^{57}\text{Fe}$  atoms at sites belonging to  $\alpha\text{-Fe}$ , CoFe, and CoFe–Mn. All spectra indicate a fully in-plane Fe spin texture. Up to  $T_S = 225^\circ\text{C}$  the spectra reveal sharp Fe/IrMn interfaces with no sign of interdiffusion. Generally, annealing up to  $225^\circ\text{C}$  led to sharper sextets, indicating an enhancement of magnetic uniformity and crystallographic order. Clear indication of interdiffusion appear only for  $T_S$  higher than  $350^\circ\text{C}$ , when it is evident the onset of non-magnetic/low magnetic hyperfine field ( $B_{\text{HF}} < 10\text{ T}$ ) components in the spectra (broad central peak). These components are attributed to both  $^{57}\text{Fe}$  atoms diffusing into the IrMn (Ta). The diffusion of Mn atoms into the  $^{57}\text{Fe}+\text{CoFe}$  layer appears as a small reduction of the magnetic splitting of the high magnetic hyperfine field components with increasing  $T_S$ .

The degree of diffusion of the  $^{57}\text{Fe}$  atoms can be estimated from the evolution of the relative intensity (spectral area) of the low field/non-magnetic components (central peak) of the Mössbauer spectra. This quantification results that, at  $450^\circ\text{C}$ , the Fe interdiffusion is  $\sim 30\%$  more pronounced at the interface than 20 Å away from the F/AF interface, as evidenced in Fig. 7.

Magnetic hysteresis loops obtained from VSM measurements after field cooling from  $T_S$  to RT are shown in Fig. 8(a). The values of  $H_E$  and coercivity ( $H_C$ ) are plotted as a function of  $T_S$  in Fig. 8(b). Interestingly, despite interdiffusion,  $H_E$  and also  $H_C$  increase with  $T_S$  up to  $450^\circ\text{C}$ . Above this temperature, there is a considerable reduction of  $H_E$  and  $H_C$ . Annealing above  $225^\circ\text{C}$  results in an enhancement of  $H_E$  due to an increase of the fraction of stable AF grains, and it seems clear that the  $H_C$  enhancement is linked to the degree of order in the AF layer, mediated by interfacial spin clusters which may acquire magnetic configurations dependent on the magnetic annealing. Such cluster configurations provide energy minima which control  $H_C$  similarly to pinning sites, i.e., the enhancement of  $H_C$  reflects a combination of bulk and interfacial effects [34,35], as discussed in details in Ref. [27].

From our results, we infer that some chemical intermixing at the interface may favor the setting of a spin configuration that increases  $H_E$ . However, heavy interdiffusion results in the destruction of magnetic order at the interfaces, and also inside the F bulk. In conclusion, at intermediate setting temperatures ( $350^\circ\text{C}$  to  $450^\circ\text{C}$ ), interfacial spin order is dominant over chemical intermixing effects, and both exchange bias field and coercivity increase up to  $T_S$  of  $450^\circ\text{C}$ . Above this temperature, heavy interdiffusion breaks the exchange coupling. After annealing at  $500^\circ\text{C}$ , surprisingly, even though the sample presented strong interdiffusion through the whole F/AF stack, as shown by CEMS, despite the abrupt reduction of  $H_E$ , a significant value of  $-250\text{ Oe}$  is still observed for this inherently interfacial coupling effect.

#### 4. Interface sharpness in epitaxial FeCo on Rh(0 0 1)

By the combination of growing FeCo/Rh(0 0 1) samples with tracer layers of  $^{57}\text{FeCo}$  with CEMS measurements, it was possible to map the spin texture of Fe atoms in epitaxial FeCo ultrathin films in a depth-selective way, and to determine how sharp is the FeCo/Rh interface [36].

Magnetic nanostructures with large uniaxial magnetocrystalline anisotropy are promising materials for perpendicular magnetic recording and other new spintronic devices [37,38]. Tetragonally distorted  $\text{Fe}_{1-x}\text{Co}_x$  alloy films epitaxially grown on different face centered cubic substrates (Pd, Pt, Ir, Rh) are a model system for perpendicular magnetic anisotropy (PMA), since, depending on the level of tetragonal distortion in the system, the epitaxy can result in strong PMA [37–42]. Distorted  $\text{Fe}_{1-x}\text{Co}_x$  films on Rh(0 0 1) show PMA in a broad composition and thickness (up to 15 ML) range, even at RT [38–40], being of high importance for applications. For systems of interest for spintronics, one important aspect is the quality of the F/substrate interface. It is shown here results on CEMS investigation of the sharpness of the epitaxial FeCo/Rh(0 0 1) interface.

FeCo films were grown on Rh(0 0 1) by co-deposition of Fe (natural Fe and  $^{57}\text{Fe}$ , 95.5% enrichment) and Co of high purity, under molecular beam epitaxy (MBE) conditions, by using two electron beam evaporators and a typical deposition rate of 1–2 ML/min. The substrate was kept at room temperature (RT). The alloy film composition was controlled by adjusting manually the individual deposition rates. The typical pressure during deposition was  $5 \times 10^{-10}\text{ mbar}$  (base pressure =  $2 \times 10^{-10}\text{ mbar}$ ). The FeCo films were always 12 monolayers (ML) thick. 4 ML  $^{57}\text{FeCo}$  was grown directly at the Rh surface, or away from the FeCo/Rh(0 0 1)

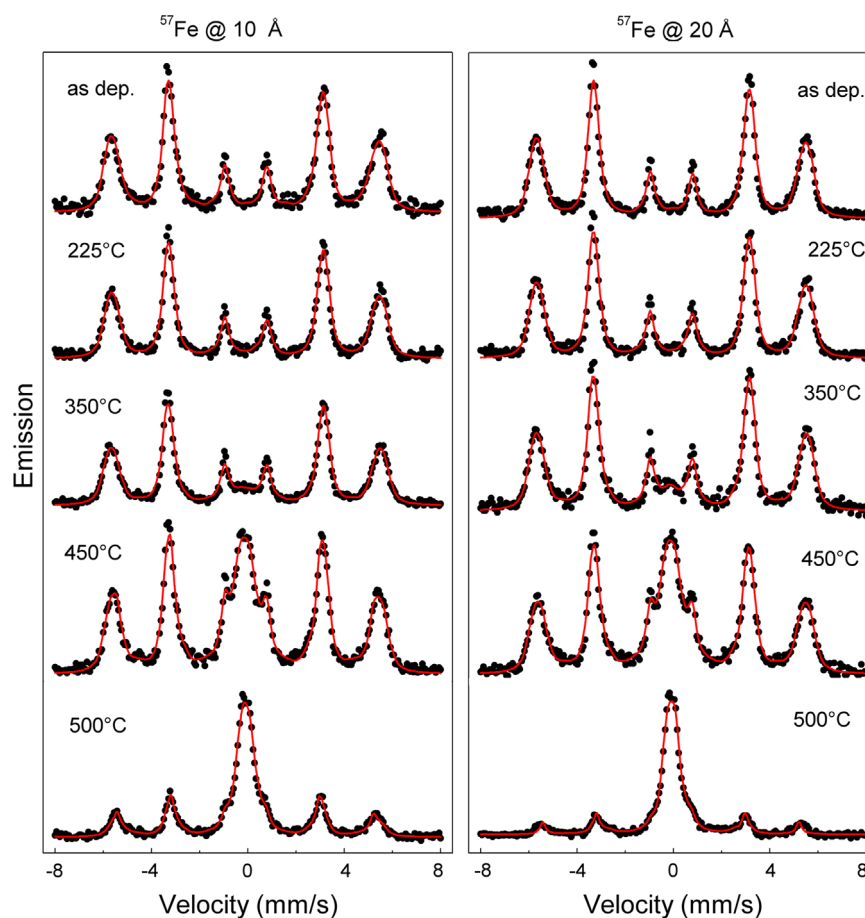


**Fig. 6.** RT CEM spectra for the  $^{57}\text{Fe}+\text{FeCo}/\text{IrMn}$  samples with the  $^{57}\text{Fe}$  probe layer 10 Å and 20 Å away from the interface. The magnetic annealing temperatures are indicated (adapted from Ref. [27]).

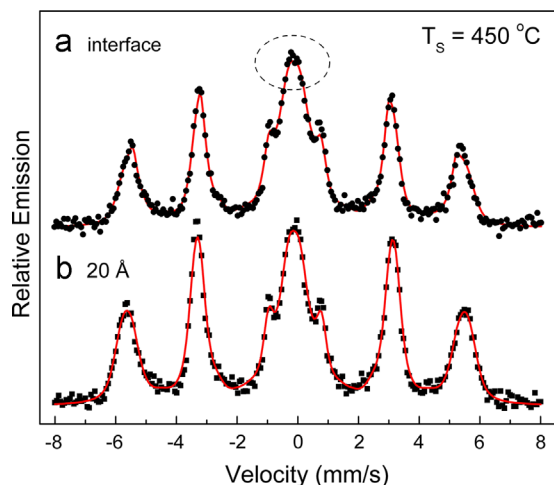


**Fig. 7.** Comparison of RT CEM spectra for  $^{57}\text{Fe}+\text{FeCo}/\text{IrMn}$  samples with (a)  $^{57}\text{Fe}$  at the interface, and (b)  $^{57}\text{Fe}$  20 Å away, after magnetic annealing at 450 °C. The evidence of higher interdiffusion at the interface is pointed out by the circle (see text).

interface, and covered with Cu or Rh layers, to prevent oxidation. We show here the investigation of the sharpness of the FeCo/Rh (0 0 1) interface.

The cleanliness of the Rh(0 0 1) substrate and the composition of the FeCo samples were examined by X-ray photoemission spectroscopy (XPS) and Auger electron spectroscopy (AES). Low energy electron diffraction (LEED) was used to probe the structure and quality of the samples. The magnetic properties of the FeCo/Rh

films were studied by MOKE in the longitudinal geometry, and by CEMS. The MOKE measurements were conducted in situ, in UHV conditions and at different temperatures, in a set-up with enough sensitivity to detect magnetization of 1 ML Fe. The maximum magnetic field at the sample, corresponding to a current of 5 A applied to the electromagnet inside the chamber, is limited to ca. 800 Oe, and the lowest sample temperature obtained by flowing liquid nitrogen through the sample manipulator was  $\sim 190$  K. The CEMS measurements were conducted ex-situ, at RT.

The LEED patterns at 62 eV for the Rh(1 0 0) substrate and for a 8 ML thick FeCo are shown in Fig. 9(a) and (b), respectively, indicating the epitaxial growth of our FeCo films on the well-ordered Rh(0 0 1) surface at RT. AES spectra (not shown) were taken immediately after the growth of 4 ML  $^{57}\text{FeCo}$  on the Rh(0 0 1) substrate, and after the deposition of additional 8 ML FeCo. The analysis of the peak-to-peak intensities of the Fe line at 700 eV and the Co line at 760 eV indicates that the films present a Fe:Co atomic concentration very close (within  $\pm 5$  at%) to the nominal composition of 50–50%.

Fig. 10 shows (a) the schematic diagram and (b) the RT CEM spectrum for a 12 ML FeCo film with 4 ML  $^{57}\text{FeCo}$  grown directly at the interface, on the Rh(0 0 1) substrate. The spectrum was fitted with two magnetic hyperfine field ( $B_{\text{HF}}$ ) distribution blocks. The main spectral contribution (blue components in color, online) corresponds to the fct FeCo alloy, with isomer shift  $\delta=0.00$  mm/s, average  $B_{\text{HF}}$  of  $34.3 \pm 0.2$  T and line intensity ratio  $R_{23}$  equal to zero (no 2 and 5 lines!), indicating fully perpendicular Fe spins in the  $^{57}\text{FeCo}$  layer, in agreement with previous MOKE magnetometry results [40–42]. These Mössbauer parameters are similar to bcc FeCo [43,44]. The second distribution block (red components in color, online), with

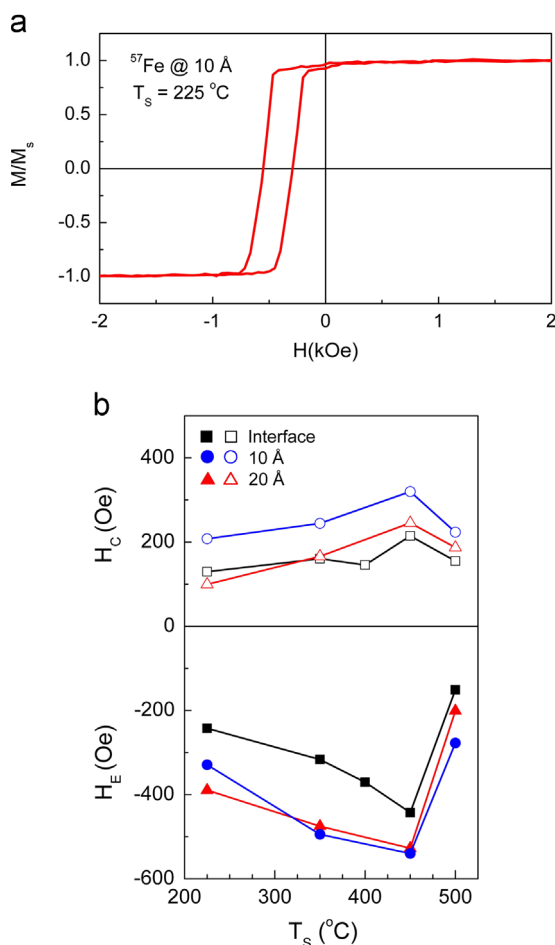


**Fig. 8.** (a) Typical magnetization loop at RT for a  $^{57}\text{Fe} + \text{FeCo}/\text{IrMn}$  bilayer annealed at  $225^\circ\text{C}$ , measured after in-plane field cooling at 3 kOe, from  $T_s$  to RT. (b) RT exchange bias field ( $H_E$ ), and coercivity ( $H_C$ ) as a function of the magnetic annealing temperature  $T_s$ , for the different series of  $^{57}\text{Fe} + \text{FeCo}/\text{IrMn}$  bilayers (adapted from Ref. [27]).

reduced magnetic hyperfine fields (average  $B_{\text{HF}} \sim 27.5 \pm 0.2$  T), amounts 30% of the spectral area, and corresponds to the very  $^{57}\text{FeCo}/\text{Rh}(1\ 0\ 0)$  interface, with some  $^{57}\text{Fe}$  atoms diffused into the Rh substrate [45], being equivalent to a thickness of 1.2 ML  $^{57}\text{FeCo}$ . For this component, despite the noise, the resulting line intensity ratio  $R_{23} \sim 0.2$  suggests a small deviation from fully perpendicular Fe spins, perhaps due to partial loss of coherence of Fe atoms in the Rh substrate.

The obtained CEMS results for RT-grown  $\text{Fe}_{50}\text{Co}_{50}/\text{Rh}(0\ 0\ 1)$  indicate that the first 4 ML present fully perpendicular spin texture and a chemically sharp interface, with very small intermixing. Moreover, the obtained values of magnetic hyperfine fields at RT for this relatively thin FeCo layer (12 ML) confirm that the Curie temperature of such films is rather high. Results on the depth-selective spin texture of Fe atoms in this epitaxial system will be presented elsewhere [36].

## 5. Summary

In this paper, three depth-resolved studies of layered magnetic nanostructures using ultrathin  $^{57}\text{Fe}$  probe layers and isotope-selective measurements by the application of CEMS and NRS techniques were briefly described. This approach is particularly important for depth-dependent analysis of buried layers, can give significant contribution for a better understanding of the structure

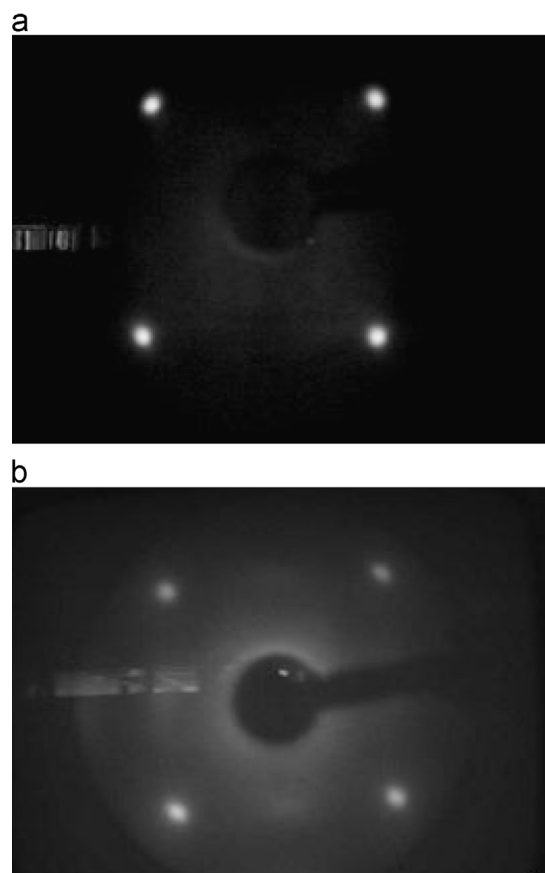


**Fig. 9.** LEED patterns at 62 eV (a) for the Rh(001) surface and (b) for 8 ML FeCo codeposited on the Rh(001) substrate at RT.

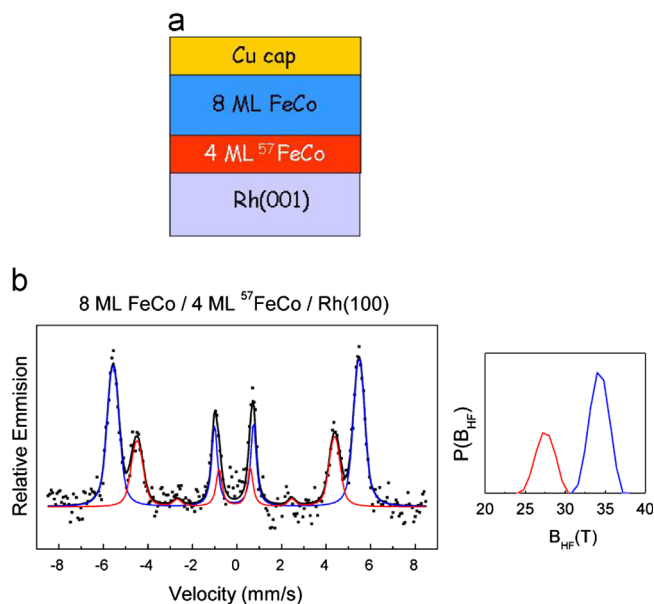


**Fig. 10.** (a) Schematic illustration of the epitaxial  $\text{FeCo}/^{57}\text{FeCo}/\text{Rh}(001)$  sample. (b) RT CEM spectrum for 12 ML FeCo/Rh(001) with 4 ML  $^{57}\text{FeCo}$  directly at the interface, and the respective magnetic hyperfine field distribution  $P(B_{\text{HF}})$ .

—magnetism correlation in nanostructured magnetic materials, and is expected to be more frequently applied in this research field, especially with the availability of new beam lines for NRS and also for synchrotron-radiation-based MS.

## Acknowledgements

The work presented in this paper was done with the fundamental participation principally from L. E. Fernandez-Outon, M. D. Martins and P. L. Gastelois, in the author's group at CDTN, in Belo Horizonte, and in strong collaboration with W. Keune and his former Ph. D. student B. Sahoo, in Duisburg, I. Schuller and collaborators, in San Diego, and M. Przybylski and J. Kirschner, from MPI in Halle. This work was financially supported by the Brazilian agencies CNPq (304368/2010-5), CAPES (CAPES/PNPD 02877/09-0) and FAPEMIG (CEX-275-04).

## References

- [1] S.D. Bader, S.S.P. Parkin, *Annu. Rev. Condens. Matter Phys.* 1 (2010) 71.
- [2] W. Keune, *Hyperfine Interact.* 27 (1986) 111.
- [3] M. Przybylski, *Hyperfine Interact.* 113 (1998) 135.
- [4] T. Shinjo, *Surf. Sci. Rep.* 12 (1991) 49.
- [5] T. Shinjo, W. Keune, *J. Magn. Magn. Mater.* 200 (1999) 598.
- [6] W. Keune, *Hyperfine Interact.* 204 (2012) 13.
- [7] R. Rohlsberger, J. Bansmann, V. Senz, K.L. Jonas, A. Bettac, O. Leupold, R. Rüffer, E. Burkel, K.H. Meiwes-Broer, *Phys. Rev. Lett.* 86 (2001) 5597.
- [8] K. Mibu, Makoto Seto, Takaya Mitsui, Yoshitaka Yoda, Ryo Masuda, Shinji Kitao, Yasuhiro Kobayashi, Edi Suharyadi, Masaaki Tanaka, Masakiyo Tsunoda, Hideto Yanagihara, Eiji Kita, *Hyperfine Interact.* 217 (2013) 127.
- [9] W.A.A. Macedo, B. Sahoo, J. Eisenmenger, M.D. Martins, W. Keune, V. Kuncser, R. Rohlsberger, O. Leupold, R. Rüffer, J. Nogués, Kai Liu, K. Schlage, Ivan K. Schuller, *Phys. Rev. B: Condens. Matter* 78 (2008) 224401.
- [10] J. Nogués, I.K. Schuller, *J. Magn. Magn. Mater.* 192 (1999) 203.
- [11] A.E. Berkowitz, K. Takano, *J. Magn. Magn. Mater.* 200 (1999) 552.
- [12] M. Kiwi, *J. Magn. Magn. Mater.* 234 (2001) 584.
- [13] F. Radu, H. Zabel, in: S.D. Bader, H. Zabel (Eds.), *Magnetic Heterostructures*, Springer, Berlin, 2007.
- [14] S.S.P. Parkin, X. Jiang, C. Kaiser, A. Panchula, K. Roche, M.G. Samant, *Proc. IEEE* 91 (2003) 661.
- [15] T.C. Schulthess, W.H. Butler, *Phys. Rev. Lett.* 81 (1998) 4516.
- [16] R.L. Stamps, *J. Phys. D: Appl. Phys.* 33 (2000) R247.
- [17] I.N. Krivorotov, C. Leighton, J. Nogués, I.K. Schuller, E.D. Dahlberg, *Phys. Rev. B: Condens. Matter* 68 (2003) 054430.
- [18] M. Kiwi, J. Mejia-Lopez, R.D. Portugal, R. Ramirez, *Appl. Phys. Lett.* 75 (1999) 3995.
- [19] R. Morales, Z.-P. Li, O.P. Petravic, X. Batlle, I.K. Schuller, *Appl. Phys. Lett.* 89 (2006) 072504.
- [20] P. Luches, L. Pasquini, S. Benedetti, S. Valeri, R. Rüffer, F. Boscherini, *Appl. Phys. Lett.* 101 (2012) 082412.
- [21] W.A.A. Macedo, B. Sahoo, V. Kuncser, J. Eisenmenger, I. Felner, J. Nogués, K. Liu, W. Keune, I.K. Schuller, *Phys. Rev. B: Condens. Matter* 70 (2004) 224414.
- [22] B. Sahoo, W.A.A. Macedo, W. Keune, V. Kuncser, J. Eisenmenger, J. Nogués, I.K. Schuller, I. Felner, Kai Liu, R. Rohlsberger, *Hyperfine Interact.* 169 (2006) 1371.
- [23] R. Rohlsberger, J. Bansmann, V. Senz, K.L. Jonas, A. Bettac, O. Leupold, R. Rüffer, E. Sturhahn, *Hyperfine Interact.* 125 (2000) 149.
- [24] R. Rohlsberger, T. Klein, K. Schlage, O. Leupold, R. Rüffer, *Phys. Rev. B: Condens. Matter* 69 (2004) 235412.
- [25] W. Sturhahn, *Hyperfine Interact.* 125 (2000) 149.
- [26] I.N. Krivorotov, C. Leighton, J. Nogués, I.K. Schuller, E.D. Dahlberg, *Phys. Rev. B: Condens. Matter* 65 (2002) 100402(R).
- [27] L.E. Fernandez-Outon, M.S. Araújo Filho, R.E. Araújo, J.D. Ardisson, W.A. A. Macedo, *J. Appl. Phys.* 113 (2013) 17D704.
- [28] P.P. Freitas, R. Ferreira, S. Cardoso, F. Cardoso, *J. Phys. Condens. Matter* 19 (2007) 165221.
- [29] G.W. Anderson, M. Pakala, Y. Huai, *IEEE Trans. Magn.* 36 (2000) 2605.
- [30] E. Kerr, S. van Dijken, J.M.D. Coey, *J. Appl. Phys.* 97 (2005) 093910.
- [31] C.-G. Lee, V.S. Gorkanov, B.-H. Koo, K.-S. Shin, R.D. McMichael, W.F. Egelhoff Jr., *Physica B* 372 (2006) 350.
- [32] V. Kuncser, W. Keune, U. von Horsten, G. Schinteie, N. Stefan, P. Palade, G. Filoti, *Thin Solid Films* 518 (2010) 5981.
- [33] J. Ventura, J.M. Teixeira, E. Paz, J.S. Amaral, J.D. Costa, A. Apolinario, J.P. Araujo, S. Cardoso, R. Ferreira, P.P. Freitas, *Phys. Status Solidi RRL* 7 (2013) 676.
- [34] K. O'Grady, L.E. Fernandez-Outon, G. Vallejo-Fernandez, *J. Magn. Magn. Mater.* 322 (2010) 883.
- [35] A.E. Berkowitz, J.-I. Hong, S.K. McCall, E. Shipton, K.T. Chan, T. Leo, D.J. Smith, *Phys. Rev. B: Condens. Matter* 81 (2010) 134404.
- [36] P.L. Gastelois et al., in preparation.
- [37] T. Burkert, L. Nordstrom, O. Eriksson, O. Heinonen, *Phys. Rev. Lett.* 93 (2004) 027203.
- [38] A. Winkelmann, M. Przybylski, F. Luo, Y. Shi, J. Barthel, *Phys. Rev. Lett.* 96 (2006) 257205.
- [39] F. Luo, X.-L. Fu, A. Winkelmann, M. Przybylski, *Appl. Phys. Lett.* 91 (2007) 262512.
- [40] F. Yildiz, F. Luo, C. Tieg, R.M. Abrudan, X.-L. Fu, A. Winkelmann, M. Przybylski, J. Kirschner, *Phys. Rev. Lett.* 100 (2008) 037205.
- [41] F. Yildiz, M. Przybylski, X.D. Ma, et al., *Phys. Rev. B: Condens. Matter* 80 (2009) 064415.
- [42] F. Yildiz, M. Przybylski, J. Kirschner, *J. Appl. Phys.* 105 (2009) 07E129.
- [43] H.H. Hamdeh, B. Fultz, D.H. Pearson, *Phys. Rev. B: Condens. Matter* 39 (1989) 11233.
- [44] H. Moumeni, S. Alleg, J.M. Greneche, *J. Alloys Compd.* 386 (2005) 12.
- [45] V. Kuncser, W. Keune, B. Sahoo, E. Duman, M. Acet, F. Radu, M. Valeanu, O. Crisan, G. Filoti, *J. Magn. Magn. Mater.* 272 (2004) 348.